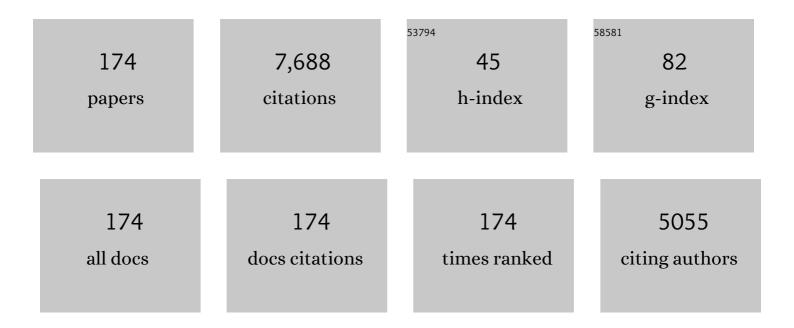
List of Publications by Year in descending order

Source: https://exaly.com/author-pdf/5598446/publications.pdf Version: 2024-02-01



#	Article	IF	CITATIONS
1	Near infrared optical tomography using NIRFAST: Algorithm for numerical model and image reconstruction. Communications in Numerical Methods in Engineering, 2009, 25, 711-732.	1.3	552
2	Intraoperative Brain Shift and Deformation: A Quantitative Analysis of Cortical Displacement in 28 Cases. Neurosurgery, 1998, 43, 749-758.	1.1	493
3	Spatially varying optical property reconstruction using a finite element diffusion equation approximation. Medical Physics, 1995, 22, 691-701.	3.0	279
4	Electromagnetic Breast Imaging: Results of a Pilot Study in Women with Abnormal Mammograms. Radiology, 2007, 243, 350-359.	7.3	278
5	Initial Clinical Experience with Microwave Breast Imaging in Women with Normal Mammography. Academic Radiology, 2007, 14, 207-218.	2.5	261
6	Imaging breast adipose and fibroglandular tissue molecular signatures by using hybrid MRI-guided near-infrared spectral tomography. Proceedings of the National Academy of Sciences of the United States of America, 2006, 103, 8828-8833.	7.1	228
7	Nonlinear Microwave Imaging for Breast-Cancer Screening Using Gauss–Newton's Method and the CGLS Inversion Algorithm. IEEE Transactions on Antennas and Propagation, 2007, 55, 2320-2331.	5.1	217
8	Initial in vivo experience with steady-state subzone-based MR elastography of the human breast. Journal of Magnetic Resonance Imaging, 2003, 17, 72-85.	3.4	202
9	Three-dimensional optical tomography: resolution in small-object imaging. Applied Optics, 2003, 42, 3117.	2.1	165
10	Local mechanical properties of white matter structures in the human brain. Neurolmage, 2013, 79, 145-152.	4.2	158
11	Three-dimensional subzone-based reconstruction algorithm for MR elastography. Magnetic Resonance in Medicine, 2001, 45, 827-837.	3.0	153
12	Quantitative fluorescence using 5-aminolevulinic acid-induced protoporphyrin IX biomarker as a surgical adjunct in low-grade glioma surgery. Journal of Neurosurgery, 2015, 123, 771-780.	1.6	131
13	Successful Translation of Fluorescence Navigation During Oncologic Surgery: A Consensus Report. Journal of Nuclear Medicine, 2016, 57, 144-150.	5.0	125
14	Modeling of Retraction and Resection for Intraoperative Updating of Images. Neurosurgery, 2001, 49, 75-85.	1.1	122
15	Electromagnetic Breast Imaging: Average Tissue Property Values in Women with Negative Clinical Findings. Radiology, 2004, 231, 571-580.	7.3	116
16	Enhanced frequency-domain optical image reconstruction in tissues through total-variation minimization. Applied Optics, 1996, 35, 3447.	2.1	107
17	Predicting Responses to Neoadjuvant Chemotherapy in Breast Cancer: ACRIN 6691 Trial of Diffuse Optical Spectroscopic Imaging. Cancer Research, 2016, 76, 5933-5944.	0.9	105
18	Magnetic resonance-guided near-infrared tomography of the breast. Review of Scientific Instruments, 2004, 75, 5262-5270.	1.3	102

#	Article	IF	CITATIONS
19	Microwave imaging for neoadjuvant chemotherapy monitoring: initial clinical experience. Breast Cancer Research, 2013, 15, R35.	5.0	98
20	Magnetic resonance elastography using 3D gradient echo measurements of steady-state motion. Medical Physics, 2001, 28, 1620-1628.	3.0	96
21	Magnetic resonance elastography of the brain using multishot spiral readouts with selfâ€navigated motion correction. Magnetic Resonance in Medicine, 2013, 70, 404-412.	3.0	93
22	Review of methods for intraoperative margin detection for breast conserving surgery. Journal of Biomedical Optics, 2018, 23, 1.	2.6	90
23	3D multislab, multishot acquisition for fast, wholeâ€brain MR elastography with high signalâ€ŧoâ€noise efficiency. Magnetic Resonance in Medicine, 2014, 71, 477-485.	3.0	84
24	Stereopsis-guided brain shift compensation. IEEE Transactions on Medical Imaging, 2005, 24, 1039-1052.	8.9	80
25	Modeling of Soft Poroelastic Tissue in Time-Harmonic MR Elastography. IEEE Transactions on Biomedical Engineering, 2009, 56, 598-608.	4.2	79
26	Image analysis methods for diffuse optical tomography. Journal of Biomedical Optics, 2006, 11, 033001.	2.6	78
27	Brain mechanical property measurement using MRE with intrinsic activation. Physics in Medicine and Biology, 2012, 57, 7275-7287.	3.0	75
28	Sub-diffusive scattering parameter maps recovered using wide-field high-frequency structured light imaging. Biomedical Optics Express, 2014, 5, 3376.	2.9	73
29	Spectral discrimination of breast pathologies in situusing spatial frequency domain imaging. Breast Cancer Research, 2013, 15, R61.	5.0	72
30	Spectral priors improve near-infrared diffuse tomography more than spatial priors. Optics Letters, 2005, 30, 1968.	3.3	71
31	Toxicity and Pharmacokinetic Profile for Single-Dose Injection of ABY-029: a Fluorescent Anti-EGFR Synthetic Affibody Molecule for Human Use. Molecular Imaging and Biology, 2017, 19, 512-521.	2.6	69
32	Parallel-detection microwave spectroscopy system for breast imaging. Review of Scientific Instruments, 2004, 75, 2305-2313.	1.3	66
33	Predicting Breast Tumor Response to Neoadjuvant Chemotherapy with Diffuse Optical Spectroscopic Tomography prior to Treatment. Clinical Cancer Research, 2014, 20, 6006-6015.	7.0	63
34	Microwave open-ended coaxial dielectric probe: interpretation of the sensing volume re-visited. BMC Medical Physics, 2014, 14, 3.	2.4	63
35	Including Spatial Information in Nonlinear Inversion MR Elastography Using Soft Prior Regularization. IEEE Transactions on Medical Imaging, 2013, 32, 1901-1909.	8.9	59
36	Magnetic Resonance Poroelastography: An Algorithm for Estimating the Mechanical Properties of Fluid-Saturated Soft Tissues. IEEE Transactions on Medical Imaging, 2010, 29, 746-755.	8.9	58

#	Article	IF	CITATIONS
37	Integration of microwave tomography with magnetic resonance for improved breast imaging. Medical Physics, 2013, 40, 103101.	3.0	58
38	Observation of direction-dependent mechanical properties in the human brain with multi-excitation MR elastography. Journal of the Mechanical Behavior of Biomedical Materials, 2016, 59, 538-546.	3.1	58
39	Contrast-detail analysis for detection and characterization with near-infrared diffuse tomography. Medical Physics, 2000, 27, 2693-2700.	3.0	56
40	Wide-field quantitative imaging of tissue microstructure using sub-diffuse spatial frequency domain imaging. Optica, 2016, 3, 613.	9.3	56
41	Hybrid element method for unbounded electromagnetic problems in hyperthermia. International Journal for Numerical Methods in Engineering, 1986, 23, 1915-1937.	2.8	53
42	Tomographic Microwave Imaging With Incorporated Prior Spatial Information. IEEE Transactions on Microwave Theory and Techniques, 2013, 61, 2129-2136.	4.6	52
43	Review of fluorescence guided surgery visualization and overlay techniques. Biomedical Optics Express, 2015, 6, 3765.	2.9	49
44	Assimilating intraoperative data with brain shift modeling using the adjoint equations. Medical Image Analysis, 2005, 9, 281-293.	11.6	48
45	Standardâ€space atlas of the viscoelastic properties of the human brain. Human Brain Mapping, 2020, 41, 5282-5300.	3.6	48
46	System analysis of spatial frequency domain imaging for quantitative mapping of surgically resected breast tissues. Journal of Biomedical Optics, 2013, 18, 036012.	2.6	47
47	Log transformation benefits parameter estimation in microwave tomographic imaging. Medical Physics, 2007, 34, 2014-2023.	3.0	46
48	Direct regularization from co-registered anatomical images for MRI-guided near-infrared spectral tomographic image reconstruction. Biomedical Optics Express, 2015, 6, 3618.	2.9	43
49	Surface Wave Multipath Signals in Near-Field Microwave Imaging. International Journal of Biomedical Imaging, 2012, 2012, 1-11.	3.9	42
50	Imaging the shear modulus of the heel fat pads. Clinical Biomechanics, 2005, 20, 312-319.	1.2	41
51	Cortical surface shift estimation using stereovision and optical flow motion tracking via projection image registration. Medical Image Analysis, 2014, 18, 1169-1183.	11.6	41
52	Performance assessment of diffuse optical spectroscopic imaging instruments in a 2-year multicenter breast cancer trial. Journal of Biomedical Optics, 2017, 22, 1.	2.6	41
53	3D microwave tomography of the breast using prior anatomical information. Medical Physics, 2016, 43, 1933-1944.	3.0	40
54	Differences in Regional Brain Volumes Two Months and One Year after Mild Traumatic Brain Injury. Journal of Neurotrauma, 2016, 33, 29-34.	3.4	39

#	Article	IF	CITATIONS
55	Implicit and explicit prior information in near-infrared spectral imaging: accuracy, quantification and diagnostic value. Philosophical Transactions Series A, Mathematical, Physical, and Engineering Sciences, 2011, 369, 4531-4557.	3.4	36
56	Simultaneous <i>In Vivo</i> Fluorescent Markers for Perfusion, Protoporphyrin Metabolism, and EGFR Expression for Optically Guided Identification of Orthotopic Glioma. Clinical Cancer Research, 2017, 23, 2203-2212.	7.0	36
57	Methodology development for three-dimensional MR-guided near infrared spectroscopy of breast tumors. Optics Express, 2008, 16, 17903.	3.4	34
58	Fluorescent Affibody Molecule Administered In Vivo at a Microdose Level Labels EGFR Expressing Glioma Tumor Regions. Molecular Imaging and Biology, 2017, 19, 41-48.	2.6	34
59	Twoâ€step inversion with a logarithmic transformation for microwave breast imaging. Medical Physics, 2017, 44, 4239-4251.	3.0	34
60	Von Neumann stability analysis of Biot's general two-dimensional theory of consolidation. International Journal for Numerical Methods in Engineering, 1998, 43, 955-974.	2.8	32
61	Hybrid photomultiplier tube and photodiode parallel detection array for wideband optical spectroscopy of the breast guided by magnetic resonance imaging. Journal of Biomedical Optics, 2013, 19, 011010.	2.6	32
62	Application of Fluorescence-Guided Surgery to Subsurface Cancers Requiring Wide Local Excision. Cancer Control, 2018, 25, 107327481775233.	1.8	32
63	Tissue oxygen saturation predicts response to breast cancer neoadjuvant chemotherapy within 10 days of treatment. Journal of Biomedical Optics, 2018, 24, 1.	2.6	32
64	Frequency-domain near-infrared photo diffusion imaging: Initial evaluation in multitarget tissuelike phantoms. Medical Physics, 1998, 25, 183-193.	3.0	31
65	A two-stage microwave image reconstruction procedure for improved internal feature extraction. Medical Physics, 2001, 28, 2358-2369.	3.0	31
66	Contrast detection in fluidâ€saturated media with magnetic resonance poroelastography. Medical Physics, 2010, 37, 3518-3526.	3.0	31
67	Brain–skull contact boundary conditions in an inverse computational deformation model. Medical Image Analysis, 2009, 13, 659-672.	11.6	30
68	3-D Microwave Tomography Using the Soft Prior Regularization Technique: Evaluation in Anatomically Realistic MRI-Derived Numerical Breast Phantoms. IEEE Transactions on Biomedical Engineering, 2019, 66, 2566-2575.	4.2	30
69	MR-Guided Near-Infrared Spectral Tomography Increases Diagnostic Performance of Breast MRI. Clinical Cancer Research, 2015, 21, 3906-3912.	7.0	29
70	Fluorescenceâ€guided surgery and intervention — An <scp>AAPM</scp> emerging technology blue paper. Medical Physics, 2018, 45, 2681-2688.	3.0	29
71	Model-Updated Image-Guided Neurosurgery Using the Finite Element Method: Incorporation of the Falx Cerebri. Lecture Notes in Computer Science, 1999, 1679, 900-909.	1.3	27
72	Sensitivity of MRI-guided near-infrared spectroscopy clinical breast exam data and its impact on diagnostic performance. Biomedical Optics Express, 2014, 5, 3103.	2.9	27

#	Article	IF	CITATIONS
73	Intraoperative image updating for brain shift following dural opening. Journal of Neurosurgery, 2016, 126, 1924-1933.	1.6	27
74	Gradient-Based Optimization for Poroelastic and Viscoelastic MR Elastography. IEEE Transactions on Medical Imaging, 2017, 36, 236-250.	8.9	27
75	Comparison of no-prior and soft-prior regularization in biomedical microwave imaging. Journal of Medical Physics, 2011, 36, 159.	0.3	27
76	Preclinical imaging of epidermal growth factor receptor with ABYâ€029 in softâ€tissue sarcoma for fluorescenceâ€guided surgery and tumor detection. Journal of Surgical Oncology, 2019, 119, 1077-1086.	1.7	26
77	Microwave tomography for bone imaging. , 2011, , .		25
78	A Patient-Specific 3D-Printed Form Accurately Transfers Supine MRI-Derived Tumor Localization Information to Guide Breast-Conserving Surgery. Annals of Surgical Oncology, 2017, 24, 2950-2956.	1.5	25
79	Micro-computed tomography enables rapid surgical margin assessment during breast conserving surgery (BCS): correlation of whole BCS micro-CT readings to final histopathology. Breast Cancer Research and Treatment, 2018, 172, 587-595.	2.5	25
80	A heterogenous, time harmonic, nearly incompressible transverse isotropic finite element brain simulation platform for MR elastography. Physics in Medicine and Biology, 2021, 66, 055029.	3.0	25
81	Structured light scatteroscopy. Journal of Biomedical Optics, 2014, 19, 070504.	2.6	24
82	Importance of phase unwrapping for the reconstruction of microwave tomographic images. Biomedical Optics Express, 2011, 2, 315.	2.9	22
83	Macroscopic optical imaging technique for wide-field estimation of fluorescence depth in optically turbid media for application in brain tumor surgical guidance. Journal of Biomedical Optics, 2015, 20, 026002.	2.6	22
84	Microdose fluorescence imaging of ABY-029 on an operating microscope adapted by custom illumination and imaging modules. Biomedical Optics Express, 2016, 7, 3280.	2.9	22
85	Methodology development for three-dimensional MR-guided near infrared spectroscopy of breast tumors. Optics Express, 2008, 16, 17903-14.	3.4	22
86	Cerebral multifrequency MR elastography by remote excitation of intracranial shear waves. NMR in Biomedicine, 2015, 28, 1426-1432.	2.8	20
87	Calibration and analysis of a multimodal micro-CT and structured light imaging system for the evaluation of excised breast tissue. Physics in Medicine and Biology, 2017, 62, 8983-9000.	3.0	20
88	Poroelastic Mechanical Properties of the Brain Tissue of Normal Pressure Hydrocephalus Patients During Lumbar Drain Treatment Using Intrinsic Actuation MR Elastography. Academic Radiology, 2021, 28, 457-466.	2.5	20
89	Adaptable Near-Infrared Spectroscopy Fiber Array for Improved Coupling to Different Breast Sizes During Clinical MRI. Academic Radiology, 2014, 21, 141-150.	2.5	19
90	Improved sensitivity to fluorescence for cancer detection in wide-field image-guided neurosurgery. Biomedical Optics Express, 2015, 6, 5063.	2.9	19

#	Article	IF	CITATIONS
91	Optimization of image reconstruction for magnetic resonance imaging–guided near-infrared diffuse optical spectroscopy in breast. Journal of Biomedical Optics, 2015, 20, 056009.	2.6	19
92	Image Updating for Brain Shift Compensation During Resection. Operative Neurosurgery, 2018, 14, 402-411.	0.8	19
93	A Randomized Prospective Trial of Supine MRI-Guided Versus Wire-Localized Lumpectomy for Breast Cancer. Annals of Surgical Oncology, 2019, 26, 3099-3108.	1.5	19
94	Initial in-vivo analysis of 3D heterogeneous brain computations for model-updated image-guided neurosurgery. Lecture Notes in Computer Science, 1998, 1496, 743-752.	1.3	18
95	Stereovision to MR image registration for cortical surface displacement mapping to enhance imageâ€guided neurosurgery. Medical Physics, 2014, 41, 102302.	3.0	18
96	Spatially-Resolved Hydraulic Conductivity Estimation Via Poroelastic Magnetic Resonance Elastography. IEEE Transactions on Medical Imaging, 2014, 33, 1373-1380.	8.9	18
97	A 4-channel, vector network analyzer microwave imaging prototype based on software defined radio technology. Review of Scientific Instruments, 2019, 90, 044708.	1.3	17
98	3D Microwave bone imaging. , 2012, , .		16
99	A numerical framework for interstitial fluid pressure imaging in poroelastic MRE. PLoS ONE, 2017, 12, e0178521.	2.5	16
100	Addition of T2-guided optical tomography improves noncontrast breast magnetic resonance imaging diagnosis. Breast Cancer Research, 2017, 19, 117.	5.0	16
101	The shape of breast cancer. Breast Cancer Research and Treatment, 2020, 183, 403-410.	2.5	16
102	First experience imaging short-wave infrared fluorescence in a large animal: indocyanine green angiography of a pig brain. Journal of Biomedical Optics, 2019, 24, 1.	2.6	16
103	MR elastography at 1â€ ⁻ Hz of gelatin phantoms using 3D or 4D acquisition. Journal of Magnetic Resonance, 2018, 296, 112-120.	2.1	15
104	Macroscopic-imaging technique for subsurface quantification of near-infrared markers during surgery. Journal of Biomedical Optics, 2015, 20, 036014.	2.6	14
105	Portable, parallel 9-wavelength near-infrared spectral tomography (NIRST) system for efficient characterization of breast cancer within the clinical oncology infusion suite. Biomedical Optics Express, 2016, 7, 2186.	2.9	14
106	Multiobjective guided priors improve the accuracy of near-infrared spectral tomography for breast imaging. Journal of Biomedical Optics, 2016, 21, 090506.	2.6	14
107	Structured light imaging for breast-conserving surgery, part II: texture analysis and classification. Journal of Biomedical Optics, 2019, 24, 1.	2.6	14
108	Measuring microdose ABY-029 fluorescence signal in a primary human soft-tissue sarcoma resection. , 2019. 10862		14

#	Article	IF	CITATIONS
109	Mapping heterogenous anisotropic tissue mechanical properties with transverse isotropic nonlinear inversion MR elastography. Medical Image Analysis, 2022, 78, 102432.	11.6	14
110	Calibration and optimization of 3D digital breast tomosynthesis guided near infrared spectral tomography. Biomedical Optics Express, 2015, 6, 4981.	2.9	13
111	Fluorescence depth estimation from wide-field optical imaging data for guiding brain tumor resection: a multi-inclusion phantom study. Biomedical Optics Express, 2017, 8, 3656.	2.9	13
112	First experience with spatial frequency domain imaging and red-light excitation of protoporphyrin IX fluorescence during tumor resection. Biomedical Optics Express, 2020, 11, 4306.	2.9	13
113	Numerical treatment of boundary conditions at points connecting more than two electrically distinct regions. Communications in Applied Numerical Methods, 1987, 3, 53-62.	0.5	12
114	Advancing molecular-guided surgery through probe development and testing in a moderate cost evaluation pipeline. Proceedings of SPIE, 2015, 9311, .	0.8	12
115	Vision 20/20: Molecularâ€guided surgical oncology based upon tumor metabolism or immunologic phenotype: Technological pathways for point of care imaging and intervention. Medical Physics, 2016, 43, 3143-3156.	3.0	12
116	Modeling and Synthesis of Breast Cancer Optical Property Signatures With Generative Models. IEEE Transactions on Medical Imaging, 2021, 40, 1687-1701.	8.9	12
117	Light scattering measured with spatial frequency domain imaging can predict stromal versus epithelial proportions in surgically resected breast tissue. Journal of Biomedical Optics, 2018, 24, 1.	2.6	12
118	Importance of phase unwrapping for the reconstruction of microwave tomographic images. Biomedical Optics Express, 2011, 2, 315-30.	2.9	12
119	Application of Linear Circuit Models to Impedance Spectra in Irradiated Musclea. Annals of the New York Academy of Sciences, 1999, 873, 21-29.	3.8	11
120	Molecular dyes used for surgical specimen margin orientation allow for intraoperative optical assessment during breast conserving surgery. Journal of Biomedical Optics, 2015, 20, 040504.	2.6	11
121	Optimizing Glioma Detection Using an EGFRâ€Targeted Fluorescent Affibody. Photochemistry and Photobiology, 2018, 94, 1167-1171.	2.5	11
122	Dualâ€agent fluorescent labeling of softâ€ŧissue sarcomas improves the contrast based upon targeting both interstitial and cellular components of the tumor milieu. Journal of Surgical Oncology, 2020, 122, 1711-1720.	1.7	11
123	Memory and operations count scaling of coupled finite-element and boundary-element systems of equations. International Journal for Numerical Methods in Engineering, 1992, 33, 1289-1303.	2.8	10
124	Cole–Cole Parameter Characterization of Urea and Potassium for Improving Dialysis Treatment Assessment. IEEE Antennas and Wireless Propagation Letters, 2012, 11, 1598-1601.	4.0	10
125	Digital breast tomosynthesis guided near infrared spectroscopy: volumetric estimates of fibroglandular fraction and breast density from tomosynthesis reconstructions. Biomedical Physics and Engineering Express, 2015, 1, 045202.	1.2	10
126	Collagen quantification in breast tissue using a 12-wavelength near infrared spectral tomography (NIRST) system. Biomedical Optics Express, 2017, 8, 4217.	2.9	10

#	Article	IF	CITATIONS
127	Hippocampal stiffness in mesial temporal lobe epilepsy measured with MR elastography: Preliminary comparison with healthy participants. NeuroImage: Clinical, 2020, 27, 102313.	2.7	10
128	Measuring protein biomarker concentrations using antibody tagged magnetic nanoparticles. Biomedical Physics and Engineering Express, 2020, 6, 065025.	1.2	10
129	Feasibility of using spatial frequency-domain imaging intraoperatively during tumor resection. Journal of Biomedical Optics, 2018, 24, 1.	2.6	10
130	Radiation boundary conditions for finite element solutions of generalized wave equations. International Journal for Numerical Methods in Fluids, 1991, 12, 765-783.	1.6	9
131	Quantitative subsurface spatial frequencyâ€domain fluorescence imaging for enhanced glioma resection. Journal of Biophotonics, 2019, 12, e201800271.	2.3	9
132	Structured light imaging for breast-conserving surgery, part I: optical scatter and color analysis. Journal of Biomedical Optics, 2019, 24, 1.	2.6	9
133	Conjugate direction methods for helmholtz problems with complex-valued wavenumbers. International Journal for Numerical Methods in Engineering, 1992, 35, 601-622.	2.8	7
134	A Contrast Source Inversion Algorithm Formulated Using the Log-Phase Formulation. International Journal of Antennas and Propagation, 2011, 2011, 1-10.	1.2	7
135	Image-derived arterial input function for quantitative fluorescence imaging of receptor-drug binding <i>in vivo</i> . Journal of Biophotonics, 2016, 9, 282-295.	2.3	7
136	Low Cost, High Performance, 16-Channel Microwave Measurement System for Tomographic Applications. Sensors, 2020, 20, 5436.	3.8	7
137	Hand-Held Stereovision System for Image Updating in Open Spine Surgery. Operative Neurosurgery, 2020, 19, 461-470.	0.8	7
138	Microwave imaging for neoadjuvant chemotherapy monitoring. , 2006, , .		6
139	Microwave tomographic imaging for breast cancer chemotherapy monitoring. , 2014, , .		6
140	Intraoperative CT as a registration benchmark for intervertebral motion compensation in image-guided open spinal surgery. International Journal of Computer Assisted Radiology and Surgery, 2015, 10, 2009-2020.	2.8	6
141	Optical scatter imaging of resected breast tumor structures matches the patterns of micro-computed tomography. Physics in Medicine and Biology, 2021, 66, 115021.	3.0	6
142	Direct Regularization From Co-Registered Contrast MRI Improves Image Quality of MRI-Guided Near-Infrared Spectral Tomography of Breast Lesions. IEEE Transactions on Medical Imaging, 2018, 37, 1247-1252.	8.9	5
143	Addressing Multipath Signal Corruption in Microwave Tomography and the Influence on System Design and Algorithm Development. Open Access Journal of Biomedical Engineering and Biosciences, 2018, 1, .	0.4	5
144	Correction to "Review of Neurosurgical Fluorescence Imaging Methodologiesâ€: IEEE Journal of Selected Topics in Quantum Electronics, 2010, 16, 1847-1847.	2.9	4

KEITH D PAULSEN

#	Article	IF	CITATIONS
145	Use of Stereovision for Intraoperative Coregistration of a Spinal Surgical Field: A Human Feasibility Study. Operative Neurosurgery, 2018, 14, 29-35.	0.8	4
146	Weighting function effects in a direct regularization method for image-guided near-infrared spectral tomography of breast cancer. Biomedical Optics Express, 2018, 9, 3266.	2.9	4
147	5-Aminolevulinic Acid-Induced Fluorescence in Focal Cortical Dysplasia: Report of 3 Cases. Operative Neurosurgery, 2019, 16, 403-414.	0.8	4
148	Comments on "Investigation of Histology Region Dielectric Measurements of Heterogeneous Tissues. IEEE Transactions on Antennas and Propagation, 2020, 68, 615-616.	5.1	4
149	Developing diagnostic assessment of breast lumpectomy tissues using radiomic and optical signatures. Scientific Reports, 2021, 11, 21832.	3.3	4
150	Model-Based Image Updating for Brain Shift in Deep Brain Stimulation Electrode Placement Surgery. IEEE Transactions on Biomedical Engineering, 2020, 67, 3542-3552.	4.2	3
151	Nonlinear Inversion MR Elastography With Low-Frequency Actuation. IEEE Transactions on Medical Imaging, 2020, 39, 1775-1784.	8.9	3
152	A level-wise spine registration framework to account for large pose changes. International Journal of Computer Assisted Radiology and Surgery, 2021, 16, 943-953.	2.8	3
153	Quantifying stability of parameter estimates for in vivo nearly incompressible transversely-isotropic brain MR elastography. Biomedical Physics and Engineering Express, 2022, 8, 035015.	1.2	3
154	Microwave Breast Imaging with a Non-Contacting, Monopole Antenna Array. , 2000, , .		2
155	Data collection strategies and their impact on 3D microwave imaging of the breast. , 2005, , .		2
156	Log transformation with Gauss-Newton microwave image reconstruction reduces incidence of local minima convergence. Digest / IEEE Antennas and Propagation Society International Symposium, 2009, , .	0.0	2
157	Bound water and the effects on tissue dielectric properties for imaging purposes. , 2014, , .		2
158	The Dartmouth Center for Cancer Nanotechnology Excellence: magnetic hyperthermia. Nanomedicine, 2015, 10, 1685-1692.	3.3	2
159	Effects of breast density and compression on normal breast tissue hemodynamics through breast tomosynthesis guided near-infrared spectral tomography. Journal of Biomedical Optics, 2016, 21, 091316.	2.6	2
160	Quantification of Subdural Electrode Shift Between Initial Implantation, Postimplantation Computed Tomography, and Subsequent Resection Surgery. Operative Neurosurgery, 2019, 16, 9-19.	0.8	2
161	MR-GUIDED PULSE OXIMETRY IMAGING OF BREAST IN VIVO. Journal of Innovative Optical Health Sciences, 2011, 04, 199-208.	1.0	1
162	Two-step reconstruction process for microwave tomography without a priori information. , 2016, , .		1

#	Article	IF	CITATIONS
163	Mathematical model to interpret localized reflectance spectra measured in the presence of a strong fluorescence marker. Journal of Biomedical Optics, 2016, 21, 061004.	2.6	1
164	Wideâ€field color imaging of scatterâ€based tissue contrast using both high spatial frequency illumination and crossâ€polarization gating. Journal of Biophotonics, 2018, 11, e201700104.	2.3	1
165	Improving the Usability of 5-Aminolevulinic Acid Fluorescence-Guided Surgery by Adding an Optimized Secondary Light Source. World Neurosurgery, 2021, 149, 195-203.e4.	1.3	1
166	Performance assessment of MRI guided continuous wave near-infrared spectral tomography for breast imaging. Biomedical Optics Express, 2021, 12, 7657.	2.9	1
167	Accuracy of Stereovision-Updated Versus Preoperative CT-Based Image Guidance in Multilevel Lumbar Pedicle Screw Placement. JBJS Open Access, 2022, 7, .	1.5	1
168	Textural analysis of optical scattering for identification of cancer in breast surgical specimens. , 2012, , .		0
169	Noninvasive bulk dielectric testing. , 2012, , .		Ο
170	ICA-guided delineation of breast cancer pathology. , 2012, , .		0
171	Effective bi-static array factor for tomographic imaging. , 2014, , .		Ο
172	Interplay between iteration step size and spatial filtering in microwave tomography. , 2016, , .		0
173	Comparison of detection sensitivity of near infrared (NIR) surgical imaging systems using a connective tissue phantom model. , 2019, 10862, .		Ο
174	A dedicated 3-ch breast coil for Microwave Tomography at 3T. Proceedings of the International Society for Magnetic Resonance in Medicine Scientific Meeting and Exhibition., 2021, 29, .	0.5	0